Attosecond delay of xenon 4*d* photoionization at the giant resonance and Cooper minimum

Maia Magrakvelidze,[1,*] Mohamed El-Amine Madjet,[2] and Himadri S. Chakraborty[1,†]

[1]*Department of Natural Sciences, D.L. Hubbard Center for Innovation and Entrepreneurship, Northwest Missouri State University, Maryville, Missouri 64468, USA*

[2]*Qatar Environment and Energy Research Institute, Hamad Bin Khalifa University, Qatar Foundation, P.O. Box 5825, Doha, Qatar*

(Received 25 May 2016; published 28 July 2016)

A Kohn-Sham time-dependent local-density-functional scheme is utilized to predict attosecond time delays of xenon 4*d* photoionization that involves the 4*d* giant dipole resonance and Cooper minimum. The fundamental effect of electron correlations to uniquely determine the delay at both regions is demonstrated. In particular, for the giant dipole resonance, the delay underpins strong collective effect, emulating the recent prediction at C_{60} giant plasmon resonance [T. Barillot *et al.*, Phys. Rev. A **91**, 033413 (2015)]. For the Cooper minimum, a qualitative similarity with a photorecombination experiment near argon 3*p* minimum [S. B. Schoun *et al.*, Phys. Rev. Lett. **112**, 153001 (2014)] is found. The result should encourage attosecond measurements of Xe 4*d* photoemission.

DOI: 10.1103/PhysRevA.94.013429

I. INTRODUCTION

Access to photoabsorption dynamics in real time via coherent pump-probe experiments is the key to fundamentally explore electron correlation processes in matter. Recent interests of such experiments [1–5] owe to the technology in generating attosecond single pulses [6,7] and pulse trains [8,9]. Of particular attraction are the experiments based on interferometric metrology, namely, the reconstruction of attosecond beating by interference of two-photon transitions (RABITT) [8], in which photoelectrons emitted by a coherent XUV comb of odd harmonics (pump) driven by a tunable fundamental field subsequently absorb or emit a synchronized infrared (IR) photon (probe). This produces even harmonic sidebands in the spectrogram which oscillate as a function of the pump-probe offset time. The ionization time delay is then obtained by the ratio of the difference of the measured phases at consecutive sidebands to the sideband separation. Since the additional delay introduced by the IR probe pulse via the so-called Coulomb-laser coupling can be estimated independently and subtracted from the measured result [10–12], this phase-energy difference approach in RABITT is commensurate with the Wigner-Smith route [13,14] to determine emission time delay that involves energy differential of the photoamplitude phase. Important recent measurements using the RABITT technique include relative delay between argon 3*s* and 3*p* photoemission [4,5], between emissions from various noble-gas atoms [15], Ar 3*p* photorecombination delay and phase at the 3*p* Cooper minimum (CM) [16], and the Ar 3*p* emission phase at a Fano autoionizing resonance [17,18].

Several theoretical methods [4,5,19–24] have been employed to explain experimental 3*s*-3*p* relative delay [4,5] in argon with a diverse range of success. Phase and Wigner-Smith delay calculations by us [24] using the time-dependent local-density approximation (TDLDA) have recently agreed very well with the experiment on argon 3*p* photorecombination around the 3*p* CM [16]. Correlated delays in the emission between atom-fullerene hybrid electrons near Cooper-type minima in the Ar@C_{60} molecule were unraveled using TDLDA [19]. For a different variety of spectral minima, which are abundant in the photoemission of cluster systems, TDLDA has probed attosecond structures in the emission delay [25]. Other successes of TDLDA include the capture of the full landscape of electronic collective motions in C_{60} driven by photons that produce experimentally detected plasmon resonances [26,27]. Very recently, TDLDA has predicted attosecond time delays of the valence photoionizations of C_{60} at the giant plasmon resonance that showed negative delay behavior over a range of the resonance, matching the outcome of a simple semiclassical modeling [28].

The Xe giant dipole resonance (GDR) in the 4*d* ionization continuum has been the focus of myriad theoretical and experimental studies over the past decades. This is a unique spectral feature largely originated from a many-body-correlation-driven collective process involving predominantly ten inner electrons in the 4*d* subshell [29–32]. This feature is fundamentally different from noncollective, large resonances, such as the $3p \rightarrow 3d$ Auger in Mn [33]. Even recently, with the advent of newer spectroscopic techniques, the Xe GDR continues to remain an eminent testing ground of many-body effects in high-order-harmonic generation (HHG) [34,35], and in applications of free electron laser in multiphoton [36] and nonlinear [37] ionization processes. On the other hand, Xe GDR can also be a particularly interesting spectral laboratory to explore the electronic temporal behavior that can discern the influence of the many-body effect on the emission time. There has only been a single measurement so far of Xe 4*d* delay relative to 5*s* by the attosecond streaking method at about 97.5 eV XUV energy [38]. Furthermore, the study of the antiresonance spectral features, such as the CM, has also been the subject of long-standing interests in both the older synchrotron-type, as in the context of Xe 4*d* CM [39,40], or the newer pump-probe RABITT spectroscopies [16]. First, the presence of such minima in pump-probe spectra indicates that the structure of the sample can be temporally probed despite the presence of an IR pulse during the process. Second, since the ionization strength significantly diminishes at the

*Present address: Department of Physics, Kansas State University, Manhattan, KS 66502, USA.

†himadri@nwmissouri.edu

vicinity of a CM, correlations with other degenerate channels become conspicuous. As a result, CM regions may serve as strategic spectral windows to scrutinize the effects of correlations [24].

In this paper, we present the phase of Xe $4d$ dipole photoionization amplitude and resulting Wigner-Smith time delay calculated in TDLDA; cross sections are presented to only compare TDLDA results with synchrotron measurements. We show how the electron-correlation-driven collective dynamics at the $4d$ GDR strongly favors an accelerated ionization of electrons by producing a negative time delay. Strong temporal variation is also found for the emission at the $4d$ CM as a consequence of the correlation. A succinct description of the method is given in Sec. II. Section III presents the numerical results with discussions. The paper is summarized in Sec. IV.

II. A BRIEF DESCRIPTION OF THEORY

Choosing the photon polarization along the z axis, the photoionization dipole transition amplitude in a single-channel independent-particle approximation, which omits electron correlations, is

$$d(\mathbf{k}) = \langle \psi_{\mathbf{k}l'} | z | \phi_{nl} \rangle. \tag{1}$$

Here $\mathbf{k}$ is the momentum of the continuum electron, z is the one-body dipole operator, ϕ_{nl} is the bound wave function of the target, and the outgoing spherical continuum wave function $\psi_{\mathbf{k}l'}$ is

$$\psi_{\mathbf{k}l'}(\mathbf{r}) = (8\pi)^{3/2} \sum_m e^{-i\eta_{l'}} R_{kl'}(r) Y_{l'm}(\Omega_{\mathbf{r}}) Y^*_{l'm}(\Omega_{\mathbf{k}}) \tag{2}$$

with $l' = l \pm 1$. In Eq. (2), the scattering phase $\eta_{l'}(k)$ contains contributions from both short-range and Coulomb potentials, besides a constant phase $l'\pi/2$, and $R_{kl'}$ is the radial continuum wave.

We calculate the amplitudes d [Eq. (1)] using the independent particle local-density approximation (LDA) method [41–43]. Here the LDA potential, using the single-particle density $\rho(\mathbf{r})$,

$$V_{\mathrm{LDA}}(\mathbf{r}) = -\frac{z}{r} + \int d\mathbf{r}' \frac{\rho(\mathbf{r}')}{|\mathbf{r} - \mathbf{r}'|} + V_{\mathrm{XC}}[\rho(\mathbf{r})], \tag{3}$$

uses the van Leeuwen–Baerends exchange-correlation functional V_{XC} [44], which provides an accurate asymptotic description of the ground-state potential. LDA self-consistently includes an average interaction with the ionic core, and obtains the ground and continuum single-electron properties for various angular momenta in a mean-field approach. Thus, LDA is akin to the Hartree-Fock method, albeit an approximation to the (nonlocal) exchange in a local frame.

TDLDA, used here to calculate the full transition amplitude, includes many-electron effects and utilizes the advanced Green's function G [43,45,46]. In a linear response frame, such as TDLDA, the photoionization amplitude formally reads

$$D(\mathbf{k}) = \langle \psi_{\mathbf{k}l'} | \delta V(\mathbf{r}) + z | \phi_{nl} \rangle = d(\mathbf{k}) + \langle \delta V(\mathbf{r}) \rangle. \tag{4}$$

Here $\delta V(\mathbf{r})$ is the energy-dependent complex induced potential that accounts for electron correlations. In TDLDA, $z + \delta V(\mathbf{r})$ is proportional to the induced frequency-dependent changes in the electron density [27]. This change is

$$\delta\rho(\mathbf{r}';\omega) = \int \chi(\mathbf{r},\mathbf{r}';\omega) z \, d\mathbf{r}, \tag{5}$$

where the full susceptibility χ builds the dynamical correlation from the independent-particle LDA susceptibilities

$$\chi^0(\mathbf{r},\mathbf{r}';\omega) = \sum_{nl}^{\mathrm{occ}} \phi^*_{nl}(\mathbf{r}) \phi_{nl}(\mathbf{r}') \, G(\mathbf{r},\mathbf{r}';\epsilon_{nl} + \omega) + \sum_{nl}^{\mathrm{occ}} \phi_{nl}(\mathbf{r}) \phi^*_{nl}(\mathbf{r}') \, G^*(\mathbf{r},\mathbf{r}';\epsilon_{nl} - \omega) \tag{6}$$

through the matrix equation $\chi = \chi^0[1 - (\partial V/\partial\rho)\chi^0]^{-1}$ involving the variation of the ground-state potential V with respect to the ground-state density ρ. The radial components of the full Green's functions in Eq. (6) are constructed with the regular (f_L) and irregular (g_L) solutions of the homogeneous radial equation

$$\left(\frac{1}{r^2} \frac{\partial}{\partial r} r^2 \frac{\partial}{\partial r} - \frac{L(L+1)}{r^2} - V_{\mathrm{LDA}} + E \right) f_L(g_L)(r;E) = 0 \tag{7}$$

as

$$G_L(r,r';E) = \frac{2 f_L(r_<;E) h_L(r_>;E)}{W[f_L,h_L]}, \tag{8}$$

where W represents the Wronskian and $h_L = g_L + i f_L$.

Using Eq. (2) in Eq. (4), the TDLDA amplitude takes the explicit form [45]

$$D(\mathbf{k}) = (8\pi)^{3/2} \sum_m C_{l'm} e^{-i\eta_{l'}} Y^*_{l'm}(\Omega_{\mathbf{k}}) \langle R_{kl'} | r + \delta V(r) | R_{nl} \rangle, \tag{9}$$

where R_{nl} is the radial bound wave function and $C_{l'm}$ includes angular momentum Wigner coefficients. Obviously, choosing $\delta V = 0$ in the TDLDA radial matrix element $\langle R_{kl'} | r + \delta V(r) | R_{nl} \rangle$ in Eq. (9) gives the LDA amplitude [Eq. (1)] involving the LDA matrix element $\langle R_{kl'} | r | R_{nl} \rangle$. The total nl cross section $\sigma_{nl} = \sum_{l'} \sigma_{nl \to kl'}$, where $\sigma_{nl \to kl'}$ is proportional to the modulus square of Eq. (9), with or without δV respectively for TDLDA and LDA, integrated over the photoelectron direction $\Omega_{\mathbf{k}}$.

The angle-resolved time delay is associated with the phase of Eq. (9) for emissions at a solid angle Ω_k [47]. In a non-angle-resolved measurement, such as RABITT, the total amplitude is directly close to the $\Omega_{\mathbf{k}}$-integrated dipole matrix elements. Thus, following Ref. [24], the TDLDA nl ionization phase can be approximated by

$$\Gamma_{nl} = \arg \left[\sum_{l'} \sqrt{\sigma_{nl \to kl'}} \exp(i \Gamma_{nl \to kl'}) \right], \tag{10}$$

where $\Gamma_{nl \to kl'}$ are the phases of corresponding amplitudes [Eq. (9)], ignoring the spherical harmonics. Hence, these channel phases are the sum of the scattering phase η and the phase of the radial matrix element. The energy differential of

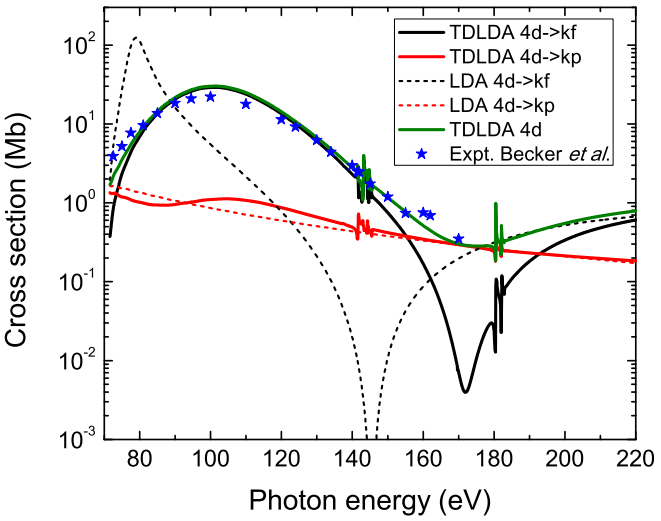

FIG. 1. LDA and TDLDA channel cross sections of the photoionization of Xe 4d. The TDLDA 4d total cross section is compared with the experiment [48].

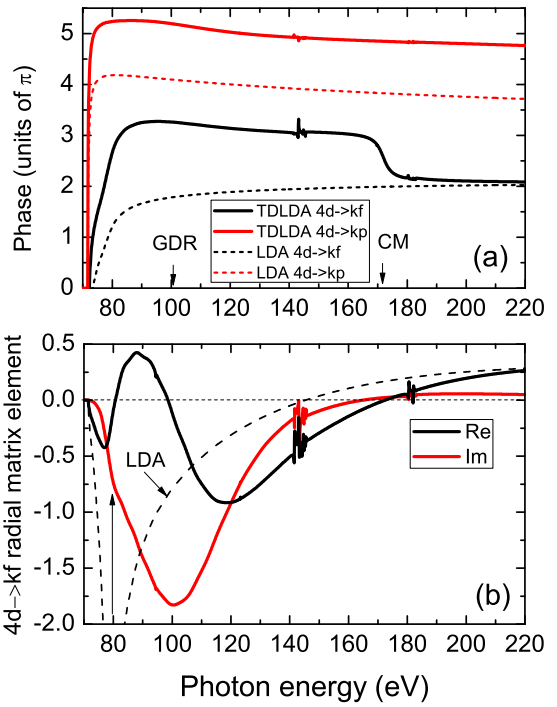

FIG. 2. (a) LDA scattering phases (η) and TDLDA phases (Γ) for the Xe 4d photoemission channels. The positions of the giant dipole resonance (GDR) at 101 eV and the Cooper minimum (CM) at 172 eV are indicated. (b) Real and imaginary components of the $4d \to kf$ radial matrix element in TDLDA where a very weak minimum at 80 eV in the imaginary part is pointed out. The real LDA radial matrix element is also shown.

Γ_{nl} is the Wigner-Smith time delay of the emission from the nl subshell [13,14]. Equation (10) and the delay derived from it recently explained $3p$ photorecombination RABITT measurements [24] very well.

III. RESULTS AND DISCUSSIONS

Figure 1 presents the LDA cross sections for the two dipole photoionization channels $4d \to kp, f$, of which the result corresponding to the kf continuum displays a shape resonance and a CM at approximately 80 and 145 eV, respectively. The origin of this shape resonance is the transient binding of the photoelectron due to the strong centrifugal barrier of the f continuum [49] and the CM is a real zero corresponding to the sign reversal of the radial LDA amplitude that is real [50]. However, as the correlation is included, that is by TDLDA, the $4d \to kp$ result is seen to remain largely unchanged, but that of $4d \to kf$ nontrivially modifies (i) the shape resonance blueshifts to 101 eV and broadens, primarily, as a consequence of the collectivization [31,51] of ten 4d electrons via the *interchannel* coupling. This resonance is known as the giant dipole resonance. (ii) The correlation in TDLDA also increases the energy of CM to 172 eV, but this minimum is now not a real zero as the imaginary component of complex δV [Eq. (4)] being nonvanishing contributes some strength at this energy. The total 4d TDLDA cross section is also presented in Fig. 1 and is compared with the experiment [48], showing very nice agreement.

We now address the phases of the 4d channels whose LDA results, the LDA scattering phases only [η in Eq. (2)], are shown in Fig. 2(a). While the lowest-energy part of these results is dominated by the long-range Coulomb phase, the short-range phase takes over at higher energies. The difference between LDA and the corresponding TDLDA results (Γ) in Fig. 2 uncovers effects of the correlation. This difference is only a constant-magnitude shift for the $4d \to kp$ channel, as seen. In contrast, the effect of correlation is rather dramatic for $4d \to kf$: The correlation switches the energy gradient of the phase from positive in LDA to negative in TDLDA over the GDR energy window and leaves its imprint across the CM by inducing a dramatic downshift of about π rad. A variation similar to the latter but for the Ar $3p \to kd$ TDLDA phase near the $3p$ CM was discussed earlier [24]. This effect transpires from the real part of the TDLDA radial matrix element sloshing through a zero at CM when the imaginary part is nonzero, as seen in Fig. 2(b). We may note that the LDA radial matrix element $\langle R_{kl'}|r|R_{nl}\rangle$ is *always* real. As a result, when it crosses a zero at CM, it produces an unphysical discontinuity in its phase due to the mathematically indeterminate arctan(0/0) right at CM. This is why only η is considered for the LDA phase. However, this is not a problem for the TDLDA matrix element, for it is complex from δV being a complex quantity and the zeros of its real and imaginary parts do not coincide in energy.

Over the GDR region, the interplay between the real and imaginary parts of the TDLDA $4d \to kf$ matrix element in Fig. 2(b) further uncovers the detailed role of correlations. As a function of energy the real part is seen to turn around and sluice through zeros twice at around 80 and 101 eV. As characteristics of the collective resonant motions [30], the imaginary component also shows minima at these energies. While this result qualitatively agrees with the time-dependent configuration interaction singles (TDCIS) calculations [32], the 80-eV minimum is found significantly weak in TDLDA

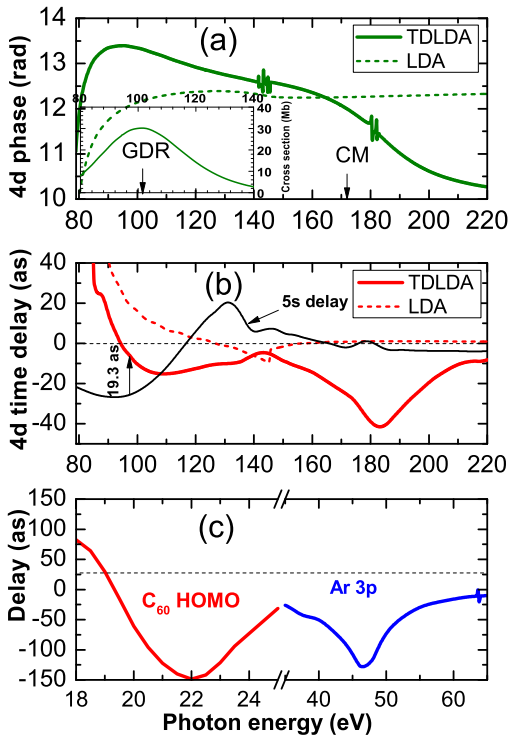

FIG. 3. (a) LDA and TDLDA 4*d* photoionization phase of Xe. The inset carries the 4*d* TDLDA cross section in the GDR region. (b) The corresponding Wigner-Smith time delays. The TDLDA delay for the $5s \rightarrow kp$ channel is also shown. The vertical arrow at 97.5 eV photon energy indicates 19.3-as TDLDA delay of the 4*d* emission relative to 5*s* which closely agrees with the relative delay of 18 as observed in streaking measurements [38]. (c) Published emission delays of the C_{60} highest occupied molecular orbital electron at the plasmon resonance [28] and Ar 3*p* electron near 3*p* CM [24], both in TDLDA, are shown for the comparison.

[Fig. 2(b)] and likely accidentally coincides with the minimum in the real LDA matrix element (shown). In contrast, the 101-eV minimum is overwhelmingly dominating in TDLDA and a focus of the current study. In fact, at the level of the TDLDA cross section (Fig. 1), which involves the squared modulus of the matrix element, the effect of the low-energy peak is obliterated. A recent study, however, shows a stronger effect of this lower minimum in the two-photon cross section [37].

Figure 3(a) presents the total 4*d* phase, in LDA [using η for Γ in Eq. (10)] and in TDLDA [using Eq. (10)] where the stronger $4d \rightarrow kf$ channel dominates. Barring the low-energy Coulomb region, the LDA phase is quite flat, producing a generally small delay in Fig. 3(b); a rather innocuous structure at 145 eV is the effect of the LDA CM in σ in Eq. (10). The TDLDA phase shows significant variations over both the GDR and CM regions. In fact, the TDLDA curve produces a broad region of negative slope, mostly over the waning part of GDR (see inset), where the effect of Coulomb repulsion weakens, resulting in a negative delay with a minimum of roughly −16 as, as Fig. 3(b) delineates. Similar negative delay times were also predicted in TDLDA for highest occupied molecular orbital (HOMO) and HOMO-1 photoemission in C_{60} at the giant plasmon resonance energies [28], which are reproduced in Fig. 3(c). This generic delay behavior at collective resonances is not surprising. When a collective excitation decays through the ionization continuum, the mechanism of the photoliberation of the electrons becomes efficient, facilitating a rather faster emission (negative delay). A possible interpretation of the Wigner-Smith delay is the excess time, positive or negative, spent by the electron to reach the continuum in addition to the time it would take in the absence of interactions between the continuum electron and the target. Hence, GDR-induced negative delay can be construed as if the emerging electrons feel a transient repulsion from its many-body interaction with the residual core that supports resonant collective motions at that particular energy. Due to the richness of many-body physics at the energies of collective response, experiments with the temporal access into Xe 4*d* giant resonance are highly desirable.

Over a wide range surrounding the 4*d* CM, TDLDA also predicts negative delays with a maximum of about −43 as at 185-eV photon energy. The result points to the considerable impact of the electron correlation via the interchannel coupling [24] of the significantly weakened 4*d* channel with other degenerate open channels around the CM. The general shape of the 4*d* phase and delay in Fig. 3 over this range agrees with those measured at Ar 3*p* CM in the photorecombination process using the RABITT technique [16], which agreed well with our TDLDA calculations [24]; the Ar 3*p* TDLDA delay is shown in Fig. 3(c) to aid comparisons. Hence, this spectral region can also be attractive for RABITT-type experiments to probe the details of electron correlation.

We also present the Xe 5*s* emission time delay result in Fig. 3(b). Since the interchannel coupling of the weaker $5s \rightarrow kp$ channel with stronger 4*d* channels clones a shape resonance in 5*s* emission as well, negative time delays in 5*s* emission induced by GDR are noted. We particularly point out that our TDLDA 4*d*-5*s* relative delay of 19.3 as at 97.5 eV closely agrees with the 18-as delay measured by the streaking spectroscopy [38].

IV. CONCLUSIONS

In conclusion, a theoretical study of Xe 4*d* photoionization spectral phases and associated Wigner-Smith time delays has been carried out within the TDLDA methodology. Strong spectral variations in the quantum phase of Xe 4*d* emission in both the 4*d* giant resonance and Cooper minimum energy ranges are noted. The Wigner-Smith time delay derived from this phase indicates a negative delay suggesting faster emission at the resonance. This is likely a ramification of efficient photoelectron emissions driven by electronic collective dynamics. The result corroborates the earlier TDLDA predictions of negative delays for the valence photoionization at the giant plasmon in C_{60} [28]. Furthermore, the phase and delay of 4*d* electrons at the 4*d* Cooper minimum suggest structures very similar to Ar 3*p* emission at its 3*p* minimum which was measured [16] and computed [24] before. TDLDA produces a reasonable comparison with the time delay detected by the streaking method for Xe 4*d* relative to the Xe 5*s* emission [38]. We hope that the current results will motivate experiments, particularly based on RABITT-type interferometric

techniques, to access temporal effects of many-body correlations near the spectrally attractive giant resonance region as well as near the correlation-sensitive Cooper minimum antiresonances.

ACKNOWLEDGMENT

The research is supported by the National Science Foundation Grant No. PHY1413799, USA.

[1] M. Schultze, M. Fieß, N. Karpowicz, J. Gagnon, M. Korbman, M. Hofstetter, S. Neppl, A. L. Cavalieri, Y. Komninos, T. Mercouris, C. A. Nicolaides, R. Pazourek, S. Nagele, J. Feist, J. Burgdörfer, A. M. Azzeer, R. Ernstorfer, R. Kienberger, U. Kleineberg, E. Goulielmakis, F. Krausz, and V. S. Yakovlev, Science **328**, 1658 (2010).

[2] S. Neppl, R. Ernstorfer, E. M. Bothschafter, A. L. Cavalieri, D. Menzel, J. V. Barth, F. Krausz, R. Kienberger, and P. Feulner, Phys. Rev. Lett. **109**, 087401 (2012).

[3] A. L. Cavalieri, N. Müller, T. Uphues, V. S. Yakovlev, A. Baltuska, B. Horvath, B. Schmidt, L. Blümel, R. Holzwarth, S. Hendel, M. Drescher, U. Kleineberg, P. M. Echenique, R. Kienberger, F. Krausz, and U. Heinzmann, Nature (London) **449**, 1029 (2007).

[4] K. Klünder, J. M. Dahlström, M. Gisselbrecht, T. Fordell, M. Swoboda, D. Guénot, P. Johnsson, J. Caillat, J. Mauritsson, A. Maquet, R. Taïeb, and A. L'Huillier, Phys. Rev. Lett. **106**, 143002 (2011).

[5] D. Guénot, K. Klünder, C. L. Arnold, D. Kroon, J. M. Dahlström, M. Miranda, T. Fordell, M. Gisselbrecht, P. Johnsson, J. Mauritsson, E. Lindroth, A. Maquet, R. Taïeb, A. L'Huillier, and A. S. Kheifets, Phys. Rev. A **85**, 053424 (2012).

[6] M. Hentschel, R. Kienberger, C. Spielmann, G. A. Reider, N. Milosevic, T. Brabec, P. Corkum, U. Heinzmann, M. Drescher, and F. Krausz, Nature (London) **414**, 509 (2001).

[7] E. Goulielmakis, M. Schultze, M. Hofstetter, V. S. Yakovlev, J. Gagnon, M. Uiberacker, A. L. Aquila, E. M. Gullikson, D. T. Attwood, R. Kienberger, F. Krausz, and U. Kleineberg, Science **320**, 1614 (2008).

[8] P. M. Paul, E. S. Toma, P. Breger, G. Mullot, F. Augé, P. Balcou, H. G. Muller, and P. Agostini, Science **292**, 1689 (2001).

[9] Y. Mairesse, A. De Bohan, L. J. Frasinski, H. Merdji, L. C. Dinu, P. Monchicourt, P. Breger, M. Kovačev, R. Taïeb, B. Carré, H. G. Muller, P. Agostini, and P. Salières, Science **302**, 1540 (2003).

[10] M. Ivanov and O. Smirnova, Phys. Rev. Lett. **107**, 213605 (2011).

[11] S. Nagele, R. Pazourek, J. Feist, and J. Burgdörfer, Phys. Rev. A **85**, 033401 (2012).

[12] J. M. Dahlström, D. Guénot, K. Klünder, M. Gisselbrecht, J. Mauritsson, A. L'Huillier, A. Maquet, and R. Taïeb, Chem. Phys. **414**, 53 (2013).

[13] E. P. Wigner, Phys. Rev. **98**, 145 (1955).

[14] F. T. Smith, Phys. Rev. **118**, 349 (1960).

[15] D. Guénot, D. Kroon, E. Balogh, E. W. Larsen, M. Kotur, M. Miranda, T. Fordell, P. Johnsson, J. Mauritsson, M. Gisselbrecht, K. Varju, C. L. Arnold, T. Carette, A. S. Kheifets, E. Lindroth, A. L'Huillier, and J. M. Dahlström, J. Phys. B **47**, 245602 (2014).

[16] S. B. Schoun, R. Chirla, J. Wheeler, C. Roedig, P. Agostini, L. F. DiMauro, K. J. Schafer, and M. B. Gaarde, Phys. Rev. Lett. **112**, 153001 (2014).

[17] Á. Jiménez-Galán, L. Argenti, and F. Martín, Phys. Rev. Lett. **113**, 263001 (2014).

[18] M. Kotur, D. Guénot, Á. Jimënez-Galán, D. Kroon, E. W. Larsen, M. Louisy, S. Bengtsson, M. Miranda, J. Mauritsson, C. L. Arnold, S. E. Canton, M. Gisselbrecht, T. Carette, J. M. Dahlström, E. Lindroth, A. Maquet, L. Argenti, F. Martín, and A. L'Huillier, Nat. Commun. **7**, 10566 (2016).

[19] G. Dixit, H. S. Chakraborty, and M. E. Madjet, Phys. Rev. Lett. **111**, 203003 (2013).

[20] J. M. Dahlström, T. Carette, and E. Lindroth, Phys. Rev. A **86**, 061402 (2012).

[21] A. S. Kheifets, Phys. Rev. A **87**, 063404 (2013).

[22] T. Carette, J. M. Dahlström, L. Argenti, and E. Lindroth, Phys. Rev. A **87**, 023420 (2013).

[23] J. M. Dahlström and E. Lindroth, J. Phys. B **47**, 124012 (2014).

[24] M. Magrakvelidze, Mohamed El-Amine Madjet, G. Dixit, M. Ivanov, and H. S. Chakraborty, Phys. Rev. A **91**, 063415 (2015).

[25] M. Magrakvelidze, D. M. Anstine, G. Dixit, Mohamed El-Amine Madjet, and H. S. Chakraborty, Phys. Rev. A **91**, 053407 (2015).

[26] S. W. J. Scully, E. D. Emmons, M. F. Gharaibeh, R. A. Phaneuf, A. L. D. Kilcoyne, A. S. Schlachter, S. Schippers, A. Müller, H. S. Chakraborty, M. E. Madjet, and J. M. Rost, Phys. Rev. Lett. **94**, 065503 (2005).

[27] M. E. Madjet, H. S. Chakraborty, J. M. Rost, and S. T. Manson, J. Phys. B **41**, 105101 (2008).

[28] T. Barillot, C. Cauchy, P.-A. Hervieux, M. Gisselbrecht, S. E. Canton, P. Johnsson, J. Laksman, E. P. Mansson, J. M. Dahlström, M. Magrakvelidze, G. Dixit, M. E. Madjet, H. S. Chakraborty, E. Suraud, P. M. Dinh, P. Wopperer, K. Hansen, V. Loriot, C. Bordas, S. Sorensen, and F. Lépine, Phys. Rev. A **91**, 033413 (2015).

[29] A. F. Starace, Phys. Rev. A **2**, 118 (1970).

[30] G. Wendin, J. Phys. B **6**, 42 (1973).

[31] M. Ya. Amusia and J. P. Connerade, Rep. Prog. Phys. **63**, 41 (2000).

[32] Yi-Jen Chen, S. Pabst, A. Karamatskou, and R. Santra, Phys. Rev. A **91**, 032503 (2015).

[33] V. K. Dolmatov, A. S. Kheifets, P. C. Deshmukh, and S. T. Manson, Phys. Rev. A **91**, 053415 (2015).

[34] A. D. Shiner, B. E. Schmidt, C. Trallero-Herrero, H. J. Worner, S. Patchkovskii, P. B. Corkum, J. C. Kieffer, F. Legare, and D. M. Villeneuve, Nat. Phys. **7**, 464 (2011).

[35] S. Pabst and R. Santra, Phys. Rev. Lett. **111**, 233005 (2013).

[36] N. Gerken, S. Klumpp, A. A. Sorokin, K. Tiedtke, M. Richter, V. Bürk, K. Mertens, P. Juranić, and M. Martins, Phys. Rev. Lett. **112**, 213002 (2014).

[37] T. Mazza, A. Karamatskou, M. Ilchen, S. Bakhtiarzadeh, A. J. Rafipoor, P. O'Keeffe, T. J. Kelly, N. Walsh, J. T. Costello, M. Meyer, and R. Santra, Nat. Commun. **6**, 6799 (2015).

[38] A. J. Verhoef, A. Mitrofanov, M. Krikunova, N. M. Kabachnik, M. Drescher, and A. Baltuska, in Proceedings of CLEO: OSA Technical Digest, Optical Society of America Paper No. QF2C.4, 2013 (unpublished).
[39] D. W. Lindle, T. A. Ferrett, P. A. Heimann, and D. A. Shirley, Phys. Rev. A **37**, 3808 (1988)
[40] N. Shanthi and P. C. Deshmukh, Phys. Rev. A **40**, 2400 (1989).
[41] M. E. Madjet, H. S. Chakraborty, and J.-M. Rost, J. Phys. B **34**, L345 (2001).
[42] M. Stener, G. De Alti, G. Fronzoni, and P. Decleva, Chem. Phys. **222**, 197 (1997).
[43] A. Zangwill and P. Soven, Phys. Rev. A **21**, 1561 (1980).
[44] R. van Leeuwen and E. J. Baerends, Phys. Rev. A **49**, 2421 (1994).
[45] W. Ekardt, Phys. Rev. B **31**, 6360 (1985).
[46] T. Nakatsukasa and K. Yabana, J. Chem. Phys. **114**, 2550 (2001).
[47] J. Wätzel, A. S. Moskalenko, Y. Pavlyukh, and J. Berakdar, J. Phys. B **48**, 025602 (2015).
[48] U. Becker, D. Szostak, H. G. Kerkhoff, M. Kupsch, B. Langer, R. Wehlitz, A. Yagishita, and T. Hayaishi, Phys. Rev. A **39**, 3902 (1989).
[49] J. W. Cooper, Phys. Rev. Lett. **13**, 762 (1964).
[50] J. W. Cooper, Phys. Rev. **128**, 681 (1962).
[51] C. Bréchignac and J. P. Connerade, J. Phys. B **27**, 3795 (1994).